Structural Engineering and Mechanics, Vol. 22, No. 6 (2006) 719-739
DOI: http://dx.doi.org/10.12989/sem.2006.22.6.719

Mode localization and veering of natural frequency loci in two circular plates coupled with a fluid

Kyeong-Hoon Jeong†

Mechanical Engineering Division, Korea Atomic Energy Research Institute,
P. O. Box 105, Yuseong, Daejeon 305-600, Republic of Korea

(Received April 28, 2005, Accepted December 13, 2005)

Abstract. An analytical method for the free vibration of two circular plates coupled with an inviscid and compressible fluid is developed by the Rayleigh-Ritz method. The fluid is bounded by a rigid cylindrical vessel and two circular plates with an unequal thickness and diameter. It was found that the theoretical results could predict well the fluid-coupled natural frequencies with an excellent accuracy when compared with the finite element analysis results. As the fluid thickness increases or the plate thickness difference increases, an abrupt curve veering in the natural frequency loci of the neighboring modes and drastic changes in the corresponding mode shapes are observed. The mode localization frequently appears in the higher modes and in the wide gap between the plates because of a decrease in the fluid coupling owing to the fluid dispersion effect.

Keywords: hydroelastic vibration; fluid-structure interaction; circular plates; mode localization; veering of natural frequency loci; Rayleigh-Ritz method.

1. Introduction

It is well known that the presence of a fluid surrounding an elastic structure reduces the natural frequency of the structure and increases the damping of the fluid-coupled system. The dynamic characteristics of the structure in contact with the fluid are one of the most fascinating problems for engineering applications. However, it is not a simple task to clearly analyze the dynamic behavior of the fluid-coupled system since the movement of the structure imparts on the fluid motion. Recently a circular plate floating on a fluid has been studied. A single circular plate in contact with a fluid has been investigated by several researchers (Amabili 1995, 1996, Amabili and Kwak 1999, Amabili 2001, Bauer 1995, Cheung and Zhou 2002, Chiba 1994, Jeong and Kim 2005, Kwak 1997, Kwak and Kim 1991, Kwak 1991, Kwak and Han 2000). On the other hand, only a few papers have focused on the dynamics of double circular plates coupled with bounded water using the Rayleigh-Ritz method (Amabili 2000, Jeong 2003). However, some discrepancies were reported in the lower modes with a zero nodal diameter because the theory was developed based on the assumption of an incompressible fluid (Jeong 2003) and the fluid-filled hermetic can problem is very complicated owing to a flexible cylindrical wall (Amabili 2000).

† Principal Researcher, E-mail: khjeong@kaeri.re.kr

This paper is motivated by the need to extend the previous study (Jeong 2003) into a more general case that can conveniently encompass the hydroelastic vibration of two arbitrary circular plates coupled with a compressible fluid. Especially, in the light water cooled nuclear reactor, it is well known that the density of the water decreases to about 70% and the bulk modulus of the water is also reduced to about 15% under a normal operational condition. Therefore, the coolant can not be considered as an incompressible fluid any more while identifying the dynamic characteristic of the reactor internals. The bottom screen assembly is one of the reactor internal components of an integrated modular nuclear reactor. The shape of the bottom screen assembly is a stack of several circular plates through gap holders. This assembly is submerged in the coolant during the normal operation and provides a shield for the reactor vessel bottom against any radiation damage due to the neutron flux from the core. This study can provide an insight into the fluid–structure interaction phenomena of the multiple circular plates submerged in a compressible fluid such as the bottom screen assembly.

Also this paper will demonstrate the existence of a mode localization and a curve veering of the natural frequency loci in the fluid-coupled circular plates. It is well known that the propagation of the vibration in nearly periodic structures can be inhibited and the vibration modes may be localized owing to small irregularities. According to the magnitude of the disorder and the strength of the internal coupling in the system, the irregularities may localize the vibration modes and confine the vibrational energy to a region close to the source. This phenomenon is referred to as a "normal mode localization" (Pierre 1988, Pierre and Dowell 1987). On the other hand, when a family of the natural frequencies is plotted versus a system parameter, the loci of the natural frequencies converge and abruptly diverge in a specific parameter region. This is called a "curve veering" (Perkins and Mote 1986). The curve veering of the natural frequency loci and the mode localization in the fluid-structure interaction problem will be investigated.

2. Theoretical formulation

2.1 Formulation for the circular plates

We investigated a system which is composed of two circular plates coupled with a fluid. The geometry of the plates needs not to be identical. The circular plates with radius R_j and thickness h_j ($<< R_j$) are fixed by the rigid cylindrical vessel with radius a as illustrated in Fig. 1. The contained fluid is in contact with the upper and the lower plates, and the fluid is bounded at $r = a$ and $x = \pm d/2$ by the rigid cylindrical vessel walls. The upper circular plate is referred to with a subscript "1" while the lower one is denoted by a subscript "2". Each wet mode shape can be expanded in a series by using a finite number of admissible functions W_{nmj} (m = 0, 1, 2, …, M; j = 1, 2), and appropriate unknown constants such as q_m and p_m. For an arbitrary nodal diameter n (n = 0, 1, 2, …) of the circular plates, the wet modal displacements w_1 and w_2 can be assumed in the form of

$$w_1(r, \theta, t) = w_1(r, \theta)\exp(i\omega t) = \cos(n\theta)\sum_{m=1}^{M} q_m W_{nm1}(r)\exp(i\omega t) \tag{1a}$$

$$w_2(r, \theta, t) = w_2(r, \theta)\exp(i\omega t) = \cos(n\theta)\sum_{m=1}^{M} p_m W_{nm2}(r)\exp(i\omega t) \tag{1b}$$

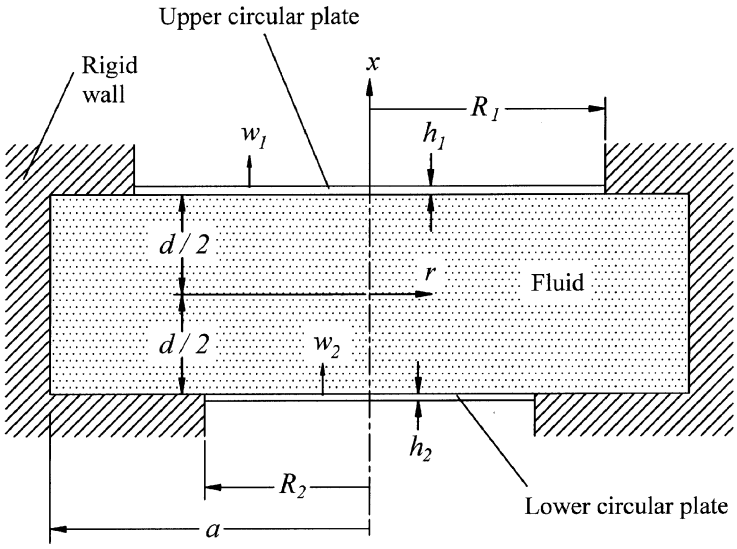

Fig. 1 Two unequal circular plates coupled with a compressible fluid

where $i = \sqrt{-1}$, ω is the fluid-coupled natural frequency of the plates and t is the time. By way of a simplicity, the eigen-functions of the plates in air which satisfy the boundary conditions along the plate edges are considered as the admissible function, $W_{nmj}(r)$. In the equation, m represents the number of nodal circles of the plates in air, at the same time it will be the number of expanding terms for the radial modal functions for the wet modes. When it is assumed that the edge of the plates are clamped, obviously the displacement of the plates at $r = R_j$ must be zero, that is, $W_{nmj} = 0$. Therefore, the admissible functions in Eqs. (1a) and (1b) can be reduced to:

$$W_{nmj}(r) = J_n(\lambda_{nm}r) - J_n(\lambda_{nm}R_j)I_n(\lambda_{nm}r)/I_n(\lambda_{nm}R_j) \tag{2}$$

Since the slope along the edge must disappear, that is, $dW_{nmj}/dr = 0$ at $r = R_j$, the frequency parameter for the plates in air, λ_{nmj}, can be calculated:

$$\frac{J_n'(\lambda_{nm}R_j)}{J_n(\lambda_{nm}R_j)} = \frac{I_n'(\lambda_{nm}R_j)}{I_n(\lambda_{nm}R_j)} \tag{3}$$

where J_n and I_n of Eqs. (2) and (3) are the Bessel function and modified Bessel function of the first kind, respectively.

2.2 Velocity and displacement potentials

As it is known that the effect of a compressibility on the natural frequencies cannot be neglected when the circular plate is coupled with water as depicted by Jeong (2003), Jeong and Kim (2005), a compressible and inviscid fluid is assumed in the theoretical formulation. The fluid between the two plates is vertically bounded by the upper and the lower rigid walls, and it is restricted by the vessel wall in the radial direction at $r = a$ as shown in Fig. 1. The oscillatory fluid flow induced by the plate motion can be described in terms of the velocity potential that satisfies the Helmholz equation:

$$\nabla^2 \Phi(r, \theta, x, t) = \Phi(r, \theta, x, t)_{,tt}/c^2 \tag{4}$$

in which c is the sound speed in the fluid medium and the comma in Eq. (4) denotes a partial derivative. It is possible to separate the velocity potential Φ with respect to r, θ and x. Thus:

$$\Phi(r, \theta, x, t) = i\omega\phi(r, \theta, x)\exp(i\omega t) = i\omega\eta(r, x)\cos(n\theta)\exp(i\omega t) \tag{5}$$

where ϕ indicates the displacement potential because the first derivative of ϕ corresponds to the dynamic displacement of the fluid. The solution of Eq. (4) for the arbitrary nodal diameter n can be derived by using a separation of the variables:

$$\phi(r, \theta, x) = \cos(n\theta)\sum_{s=1}^{\infty} J_n(\beta_{ns} r)\{E_{ns}\sinh(\alpha_{ns} x) + F_{ns}\cosh(\alpha_{ns} x)\} \tag{6}$$

where

$$\beta_{ns}^2 = \alpha_{ns}^2 + (\omega/c)^2 \tag{7}$$

Since the fluid is bounded by the rigid cylindrical wall as illustrated in Fig. 1, the radial displacement of the fluid at $r = a$ must be zero:

$$\left.\frac{\partial\phi(r, \theta, x)}{\partial r}\right|_{r=a} = 0 \tag{8}$$

Substitution of Eq. (6) into Eq. (8) gives Eq. (9) and the parameter β_{ns} can be determined with respect to every s and n:

$$J_n'(\beta_{ns} a) = 0 \tag{9}$$

2.3 Method of the solution

We assume that the fluid particles in contact with the surface of the plates are an equilibrium state, and remain so during the movement. The compatibility condition results from a slipping of the fluid, which is equivalent to the normal displacements from an instantaneous configuration of the fluid-structure contact surface being equal to:

$$\frac{\partial\phi(r, \theta, d/2)}{\partial x} = \begin{cases} w_1(r, \theta), & 0 \le r \le R_1 \\ 0, & R_1 < r \le a \end{cases} \tag{10a}$$

$$\frac{\partial\phi(r, \theta, -d/2)}{\partial x} = \begin{cases} w_2(r, \theta), & 0 \le r \le R_2 \\ 0, & R_2 < r \le a \end{cases} \tag{10b}$$

The unknown coefficients E_{ns} and F_{ns} of Eq. (6) describing the fluid motion can be determined when the above two compatibility conditions are considered. Substitution of Eqs. (1a), (1b), (2), (6) into Eqs. (10a) and (10b) gives;

$$\sum_{s=1}^{\infty} \alpha_{ns}[E_{ns}\cosh(\alpha_{ns}d/2) + F_{ns}\sinh(\alpha_{ns}d/2)]J_n(\beta_{ns}r)$$

$$= \begin{cases} \sum_{m=1}^{M} q_m[J_n(\lambda_{nm}r) - J_n(\lambda_{nm}R_1)I_n(\lambda_{nm}r)/I_n(\lambda_{nm}R_1)], & 0 \le r \le R_1 \\ 0, & R_1 < r \le a \end{cases} \tag{11a}$$

$$\sum_{s=1}^{\infty} \alpha_{ns}[E_{ns}\cosh(\alpha_{ns}d/2) - F_{ns}\sinh(\alpha_{ns}d/2)]J_n(\beta_{ns}r)$$

$$= \begin{cases} \sum_{m=1}^{M} p_m[J_n(\lambda_{nm}r) - J_n(\lambda_{nm}R_2)I_n(\lambda_{nm}r)/I_n(\lambda_{nm}R_2)], & 0 \le r \le R_2 \\ 0, & R_2 < r \le a \end{cases} \tag{11b}$$

However, we still cannot obtain the relationship between the unknown coefficients (E_{ns} and F_{ns}) of the fluid and the modal unknown constants (q_m and p_m) directly. So we multiply each side of both equations by $rJ_n(\beta_{ns}r)$ and integrate them over their respective domains, then the equations can be obtained;

$$\int_0^{R_1} \sum_{m=1}^{M} q_m[J_n(\lambda_{nm}r) - J_n(\lambda_{nm}R_1)I_n(\lambda_{nm}r)/I_n(\lambda_{nm}R_1)]rJ_n(\beta_{ns}r)dr$$

$$= \int_0^a \sum_{s=1}^{\infty} \alpha_{ns}[E_{ns}\cosh(\alpha_{ns}d/2) + F_{ns}\sinh(\alpha_{ns}d/2)]rJ_n^2(\beta_{ns}r)dr \tag{12a}$$

$$\int_0^{R_2} \sum_{m=1}^{M} p_m[J_n(\lambda_{nm}r) - J_n(\lambda_{nm}R_2)I_n(\lambda_{nm}r)/I_n(\lambda_{nm}R_2)]rJ_n(\beta_{ns}r)dr$$

$$= \int_0^a \sum_{s=1}^{\infty} \alpha_{ns}[E_{ns}\cosh(\alpha_{ns}d/2) - F_{ns}\sinh(\alpha_{ns}d/2)]rJ_n^2(\beta_{ns}r)dr \tag{12b}$$

We integrate Eqs. (12a) and (12b) over the radius of the vessel, term by term and arrange both the equations simultaneously. Finally the unknown coefficients E_{ns} and F_{ns} can be written in terms of the unknown constants q_m and p_m.

$$E_{ns} = \frac{2\alpha_{ns}}{\sigma_{ns}\cosh(\alpha_{sn}d/2)} \sum_{m=1}^{M} \{q_m\Gamma_{nms1} + p_m\Gamma_{nms2}\} \tag{13a}$$

$$F_{ns} = \frac{2\alpha_{ns}}{\sigma_{ns}\sinh(\alpha_{sn}d/2)} \sum_{m=1}^{M} \{q_m\Gamma_{nms1} - p_m\Gamma_{nms2}\} \tag{13b}$$

$$\Gamma_{nms1} = \frac{R_1^2(\lambda_{nm}R_1)^2[(\lambda_{nm}R_1)J_n'(\lambda_{nm}R_1)J_n(\beta_{ns}R_1) - (\beta_{ns}R_1)J_n(\lambda_{nm}R_1)J_n'(\beta_{ns}R_1)]}{(\beta_{ns}R_1)^4 - (\lambda_{nm}R_1)^4} \tag{13c}$$

$$\Gamma_{nms2} = \frac{R_2^2(\lambda_{nm}R_2)^2[(\lambda_{nm}R_2)J_n'(\lambda_{nm}R_2)J_n(\beta_{ns}R_2) - (\beta_{ns}R_2)J_n(\lambda_{nm}R_2)J_n'(\beta_{ns}R_2)]}{(\beta_{ns}R_2)^4 - (\lambda_{nm}R_2)^4} \tag{13d}$$

$$\sigma_{ns} = (\alpha_{ns}a^2)\left\{1 - \frac{n^2}{(\beta_{ns}a)^2}\right\}\{J_n(\beta_{ns}a)\}^2 \tag{13e}$$

The displacement potential of the compressible fluid can now be rewritten by a substitution of Eqs. (13a)-(13e) into Eq. (6).

$$\phi(r, \theta, x) = \cos(n\theta)\sum_{m=1}^{M}\sum_{s=1}^{\infty}\{q_m N_{nms}(x) + p_m M_{nms}(x)\}J_n(\beta_{ns}r) \tag{14}$$

where

$$N_{nms}(x) = \frac{2\alpha_{ns}\Gamma_{nms1}}{\sigma_{ns}}\left\{\frac{\sinh(\alpha_{ns}x)}{\cosh(\alpha_{ns}d/2)} + \frac{\cosh(\alpha_{ns}x)}{\sinh(\alpha_{ns}d/2)}\right\} \tag{15a}$$

$$M_{nms}(x) = \frac{2\alpha_{ns}\Gamma_{nms2}}{\sigma_{ns}}\left\{\frac{\sinh(\alpha_{ns}x)}{\cosh(\alpha_{ns}d/2)} - \frac{\cosh(\alpha_{ns}x)}{\sinh(\alpha_{ns}d/2)}\right\} \tag{15b}$$

Now we apply the classical energy method to obtain the fluid-coupled natural frequencies of the two unequal circular plates coupled with the compressible fluid:

$$\omega^2 = \frac{V_p}{T_p^* + U_F^*} \tag{16}$$

where V_p and T_p^* are the potential and reference kinetic energies of the plates. The term U_F^* is the reference fluid energy term including the fluid kinetic and potential energies which can be evaluated from the surface motion of the fluid;

$$U_F^* = \frac{1}{2}\rho_o\int_0^{2\pi}\int_0^{R_1}\left(\frac{\partial\phi(r, d/2)}{\partial x}\right)\phi(r, d/2)\cos^2(n\theta)r\,dr\,d\theta$$
$$+ \frac{1}{2}\rho_o\int_0^{2\pi}\int_0^{R_2}\left(\frac{\partial\phi(r, -d/2)}{\partial x}\right)\phi(r, -d/2)\cos^2(n\theta)r\,dr\,d\theta \tag{17}$$

where ρ_o is the mass density of the compressible fluid. By substituting Eqs. (5) and (10a, b) into Eq. (17), it reduces to;

$$U_F^* = \frac{1}{2}\rho_o\kappa_\theta\left(\int_0^{R_1} w_1\,\eta(r, d/2)r\,dr + \int_0^{R_2} w_2\,\eta(r, -d/2)r\,dr\right) \tag{18}$$

where

$$\kappa_\theta = \begin{cases} 2\pi & \text{for } n = 0 \\ \pi & \text{for } n > 0 \end{cases} \tag{19}$$

The reference kinetic energy of the two circular plates, as obtained, can be expressed as;

$$T_p^* = \frac{\rho}{2}\int_0^{2\pi}\left[h_1\int_0^{R_1} w_1^2 r\,dr + h_2\int_0^{R_2} w_2^2 r\,dr\right]d\theta \tag{20}$$

where ρ is the density of the plates. The maximum potential energy of the two plates can be simplified as;

$$V_p \cong \frac{1}{2}\int_0^{2\pi}\left[D_1\int_0^{R_1}(\nabla^2 w_1)^2 r\,dr + D_2\int_0^{R_2}(\nabla^2 w_2)^2 r\,dr\right]d\theta \tag{21}$$

where $D_j = E\,h_j^3/12\,(1-\mu^2)$ is the flexural rigidity of the circular plates; μ and E are the Poisson's ratio and the modulus elasticity of the plates, respectively. Taking the variation with respect to the unknown constants q_m and p_m in order to perform the numerical calculations for each fixed n value, we can write the energies in a matrix form;

$$U_F^* = \rho_o \kappa_\theta \boldsymbol{Q}^T \boldsymbol{G} \boldsymbol{Q} \tag{22a}$$

$$T_p^* = \rho \kappa_\theta \boldsymbol{Q}^T \boldsymbol{Z} \boldsymbol{Q} \tag{22b}$$

$$V_p = \kappa_\theta \boldsymbol{Q}^T \boldsymbol{P} \boldsymbol{Q} \tag{22c}$$

The column vectors $\boldsymbol{q}$, $\boldsymbol{p}$ and $\boldsymbol{Q}$ of the unknown parameters are defined as follows:

$$\boldsymbol{q} = \{q_1 \;\; q_2 \;\; q_3 \;\; \cdots \;\; q_M\}^T \tag{23a}$$

$$\boldsymbol{p} = \{p_1 \;\; p_2 \;\; p_3 \;\; \cdots \;\; p_M\}^T \tag{23b}$$

$$\boldsymbol{Q} = \begin{Bmatrix} \boldsymbol{q} \\ \boldsymbol{p} \end{Bmatrix} \tag{23c}$$

The matrices in Eqs. (22a)-(22c) can be derived by integrations of the equations. The $2M \times 2M$ matrix $\boldsymbol{G}$ in Eq. (22a) will be written as;

$$\boldsymbol{G} = \begin{bmatrix} G1 & G2 \\ G3 & G4 \end{bmatrix} \tag{24}$$

$$G1_{ik} = 4\sum_{s=1}^{\infty}\frac{\Gamma_{nis1}}{\sigma_{ns}}\left\{\Gamma_{nks1}\tanh\left(\frac{\alpha_{ns}d}{2}\right) + \Gamma_{nks2}\cosh\left(\frac{\alpha_{ns}d}{2}\right)\right\} \tag{25a}$$

$$G2_{ik} = 4\sum_{s=1}^{\infty}\frac{\Gamma_{nis1}}{\sigma_{ns}}\left\{\Gamma_{nks1}\tanh\left(\frac{\alpha_{ns}d}{2}\right) - \Gamma_{nks2}\coth\left(\frac{\alpha_{ns}d}{2}\right)\right\} \tag{25b}$$

$$G3_{ik} = 4\sum_{s=1}^{\infty}\frac{\Gamma_{nis2}}{\sigma_{ns}}\left\{-\Gamma_{nks1}\tanh\left(\frac{\alpha_{ns}d}{2}\right) + \Gamma_{nks2}\coth\left(\frac{\alpha_{ns}d}{2}\right)\right\} \tag{25c}$$

$$G4_{ik} = -4\sum_{s=1}^{\infty}\frac{\Gamma_{nis2}}{\sigma_{ns}}\left\{\Gamma_{nks1}\tanh\left(\frac{\alpha_{ns}d}{2}\right) + \Gamma_{nks2}\coth\left(\frac{\alpha_{ns}d}{2}\right)\right\}, \;\; i,k = 1, 2, \ldots, M \tag{25d}$$

The matrix $\boldsymbol{Z}$ in Eq. (22b) is the $2M \times 2M$ matrix given as;

$$\boldsymbol{Z} = \begin{bmatrix} \boldsymbol{Z}_1 & 0 \\ 0 & \boldsymbol{Z}_2 \end{bmatrix} \tag{26}$$

$$Z_{j(i,k)} = h_j \frac{R_j^2}{2} \{J_n(\lambda_{ni} R_j)\}^2 \delta_{ik}, \quad i, k = 1, 2, \ldots, M \tag{27}$$

where δ_{ik} is the Kronecker delta. As the term $(\nabla^2 w_j)^2$ in Eq. (21) is identical to $\lambda_{ni}^4 w_j^2$, the $2M \times 2M$ diagonal matrix $\boldsymbol{P}$ in Eq. (22c) will be reduced as;

$$\boldsymbol{P} = \begin{bmatrix} \boldsymbol{P}_1 & 0 \\ 0 & \boldsymbol{P}_2 \end{bmatrix} \tag{28}$$

$$P_{j(i,k)} = \frac{D_j (\lambda_{ni} R_j)^4}{2R_j^2} \{J_n(\lambda_{ni} R_j)\}^2 \delta_{ik}, \quad i, k = 1, 2, \ldots, M \tag{29}$$

From the correspondence between the kinetic and the potential energies of the plates and the compressible fluid, the Galerkin equation can be obtained by minimizing the Rayleigh quotient with respect to the unknown parameters q_m and p_m.

$$\boldsymbol{P}\boldsymbol{Q} - \omega^2 (\rho \boldsymbol{Z} + \rho_o \boldsymbol{G}) \boldsymbol{Q} = \{0\} \tag{30}$$

In Eqs. (25a)-(25d), the sum of s must be stopped for a numerical computation, at an integer value large enough to give the required accuracy. Since the matrix $\boldsymbol{G}$ is a function of ω, Eq. (30) can not be an ordinary eigenvalue problem. Therefore, the eigenvalue problem cannot be obtained directly. The determinant of the left side in Eq. (30) must be zero to obtain the non-trivial solution.

3. Verification of the theory

3.1 Theoretical and finite element models

An example was numerically solved, because one of the aims of this analysis is to verify the proposed theoretical formulation. Initially, in order to obtain the natural frequencies of the two unequal aluminum circular plates coupled with water, theoretical calculations were carried out so that the determinant of the left side in Eq. (30) could be zero. Although Eq. (30) is not an ordinary eigenvalue problem, the calculations could be performed by using an iterating process of the commercial software, MathCAD (version 2000). The initial values were obtained from the incompressible fluid case which leads to an ordinary eigenvalue problem, and the expected frequency zone was swept to calculate the coupled natural frequencies. In the theoretical calculation, the frequency equation derived from the preceding sections involved a double series of expansions in terms of s and m. Hence the expansion term s is taken as 200 and the expanding term m for the admissible function is taken as 30 to obtain a converged solution. The geometric and the physical

Table 1 Specifications of the two fluid-coupled circular plates

	Upper plate	Lower plate	Rigid cylinder	Fluid
Radius, [mm]	$R_1 = 150.0$	$R_2 = 120.0$	$a = 180.0$	–
Thickness, [mm]	$h_1 = 3.0$	$h_2 = 2.0$	–	–
Mass density [kg/m^3]	$\rho = 2700.0$	$\rho = 2700.0$	–	$\rho_o = 1000.0$
Modulus of elasticity [GPa]	$E = 69.0$	$E = 69.0$	–	$B = 2.2$
Poisson's ratio	$\mu = 0.3$	$\mu = 0.3$	–	–
Distance between the plates [mm]	–	–	–	$d = 40.0$

properties of the fluid-coupled system are listed in Table 1.

Additionally, in order to validate the proposed theory, finite element analyses were also performed for the water-coupled system using a commercial computer code, ANSYS (release 7.0). An axisymmetric two dimensional model was constructed with the same geometry, boundary conditions and material properties used in the theoretical calculation. In the finite element analysis, the axisymmetric harmonic fluid elements (FLUID81) and axisymmetric harmonic shell elements (SHELL61) were used. The viscosity of the water was neglected both in the theoretical calculation and in the finite element analyses. The fluid domain of the finite element models was divided into 960 fluid elements and the upper and the lower plates were also discretized with 88 shell elements as illustrated in Fig. 2. The fluid movement at $r = a$ namely along the rigid cylindrical wall is only restricted in the radial direction but slips between the rigid wall and the water are allowed along the azimuthal and vertical directions. In a similar manner, an additional restriction should be imposed so that the fluid movement at $x = \pm d/2$ and $R_j \le r \le a$, namely along the rigid upper and the lower

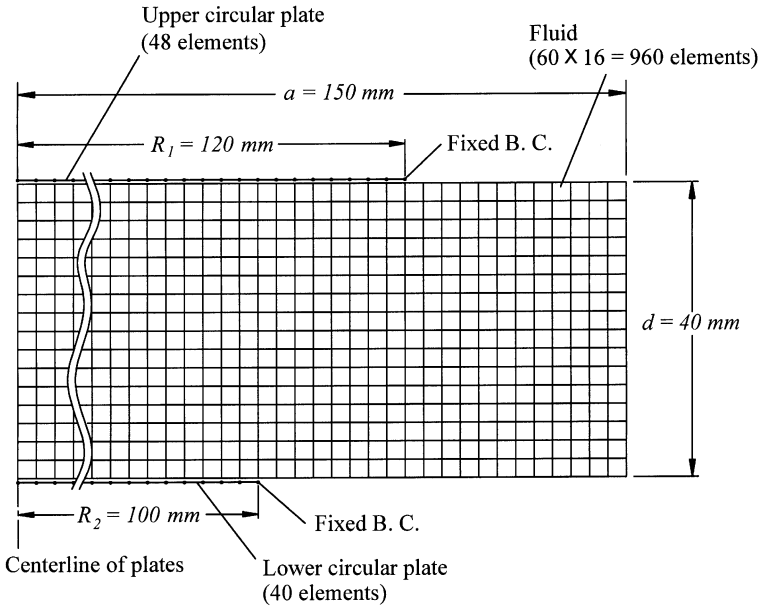

Fig. 2 Axisymmetric two dimensional finite element analysis model for two unequal aluminum circular plates coupled with water

walls can be zero in the vertical direction only, but those slips between the rigid wall and water are allowed along the azimuthal and the radial directions. These restrictions for the fluid displacement simulate Eq. (8) and the lower parts of Eqs. (10a) and (10b). The vertical displacement of the fluid element nodes adjacent to each surface of the wetted circular plates coincides with those of the circular plates so that the finite element model can simulate the compatibility condition of the upper parts of Eqs. (10a) and (10b). A fixed boundary condition along each plate edge was imposed on the finite element model. For every nodal diameter n, fifty modal frequencies and mode shapes were extracted from the frequency range of 30 Hz ~ 8000 Hz. In the finite element analyses, the reduced method was used for the eigenvalue and eigenvector extractions, which employs the Block-Lanczos extraction technique.

3.2 Theoretical and finite element results

The coupled natural frequencies for the unequal aluminum plates coupled with water are listed in Table 2 for the range of $0 \le n \le 4$ and $1 \le m' \le 6$, where the radial mode number is denoted by m'. In this range, it is shown that the theoretical natural frequencies agree well with the finite element results to within a 2.5% error range. The difference between the theoretical and the finite element natural frequencies is negligible from an engineering sense. It seems that the discrepancy is caused by the weighted integration process of Eqs. (12a) and (12b). In spite of the discrepancy, this weighted integration process is identical to the Bessel-Fourier series expansion process (Jeong 2003) when $R_1 = R_2 = a$.

When the two plates are the same in material property and geometry, all the mode shapes can be classified into two transverse vibration mode categories according to their relative motion direction between the two plates during a vibration; that is, the in-phase and the out-of-phase modes (Jeong 2003). However, it is inappropriate for all the mode shapes to be simply categorized as either in-phase or out-of-phase modes for a system with unequal plates, since they do not maintain a symmetrical in-phase and out-of-phase mode. Strictly speaking, the mode shapes can be grouped into three classes; pseudo-in-phase modes, pseudo-out-of-phase modes, and mixed modes, as shown in mode shapes A2~A6, B2~B6, …, F2~F6 of Figs. 5, 7, 9 and 11. From the verification model of Table 1, it is observed that the relative dynamic displacement difference between the two plates for the in-phase mode shapes is smaller than that of the corresponding out-of-phase mode shapes. An important point to note arises from the fact that the stiffness difference between the plates affects the out-of-phase mode shapes more than the in-phase mode shapes. Since the vertical fluid flow direction coincides with the dynamic displacement of the plates for the in-phase modes, the dynamic displacement of the stiff plate encourages the flexible plate to move in the same direction. On the contrary, for the out-of-phase modes, each plate hinders it's oppositely facing plate from moving in the opposite direction through the contained fluid. As the number of the vibration modes increases in the radial direction, the number of the nodal circles of the two plates does not match at the higher modes. These modes are called mixed modes. The mixed modes frequently appear at the higher modes when the difference in the structural stiffness of two plates is small, and they are also observed at the lower modes when the difference in the structural stiffness of two plates is large. As listed in Table 2, the first out-of-phase mode with $n = 0$ cannot appear because the vibration mode violates the fluid volume conservation.

Table 2 Comparison of the FEM and theoretical natural frequencies of the two circular plates coupled with water

Mode		Natural frequency (Hz)		Discrepancy[1)] (%)	Mode shape
n	m'	FEM	Theory		
0	1	—	—	—	—
	2	255.0	255.6	−0.24	In-phase mode
	3	688.7	674.4	2.07	Out-of-phase mode
	4	1062.3	1077.7	−1.44	In-phase mode
	5	2172.2	2119.1	2.44	Mixed mode
	6	2595.1	2651.4	−2.17	In-phase mode
1	1	275.6	275.7	−0.04	Out-of-phase mode
	2	548.6	549.7	−0.20	In-phase mode
	3	1342.2	1318.0	1.80	Out-of-phase mode
	4	1704.6	1733.4	−1.69	In-phase mode
	5	3198.5	3178.2	0.63	Out-of-phase mode
	6	3639.7	3686.3	−1.28	Mixed mode
2	1	663.9	663.8	0.02	Out-of-phase mode
	2	939.9	941.3	−0.15	In-phase mode
	3	2154.1	2131.2	0.16	Out-of-phase mode
	4	2495.1	2520.2	0.92	In-phase mode
	5	4401.8	4329.6	1.64	Out-of-phase mode
	6	4848.6	4861.8	−0.27	Mixed mode
3	1	1163.2	1163.2	0.00	Out-of-phase mode
	2	1438.7	1440.7	−0.14	In-phase mode
	3	3067.4	3051.3	0.52	Out-of-phase mode
	4	3438.0	3457.0	−0.55	In-phase mode
	5	5736.2	5688.9	0.82	Out-of-phase mode
	6	6224.2	6306.6	−1.32	Mixed mode
4	1	1761.1	1761.8	−0.04	Out-of-phase mode
	2	2052.4	2055.1	−0.13	In-phase mode
	3	4077.7	4069.0	0.21	Out-of-phase mode
	4	4521.2	4535.9	−0.33	In-phase mode
	5	7180.5	7151.3	0.41	Out-of-phase mode
	6	7749.0	7797.0	−0.62	Mixed mode

[1)]Discrepancy (%) = (FEM − Theory) × 100 / FEM

4. Mode localization and the curve veering of the natural frequency loci

4.1 Mode localization

It is well known that a disorder in nearly periodic structures tends to inhibit the propagation of a motion and to localize the vibration modes (Pierre and Dowell 1987, Pierre 1988). The mode

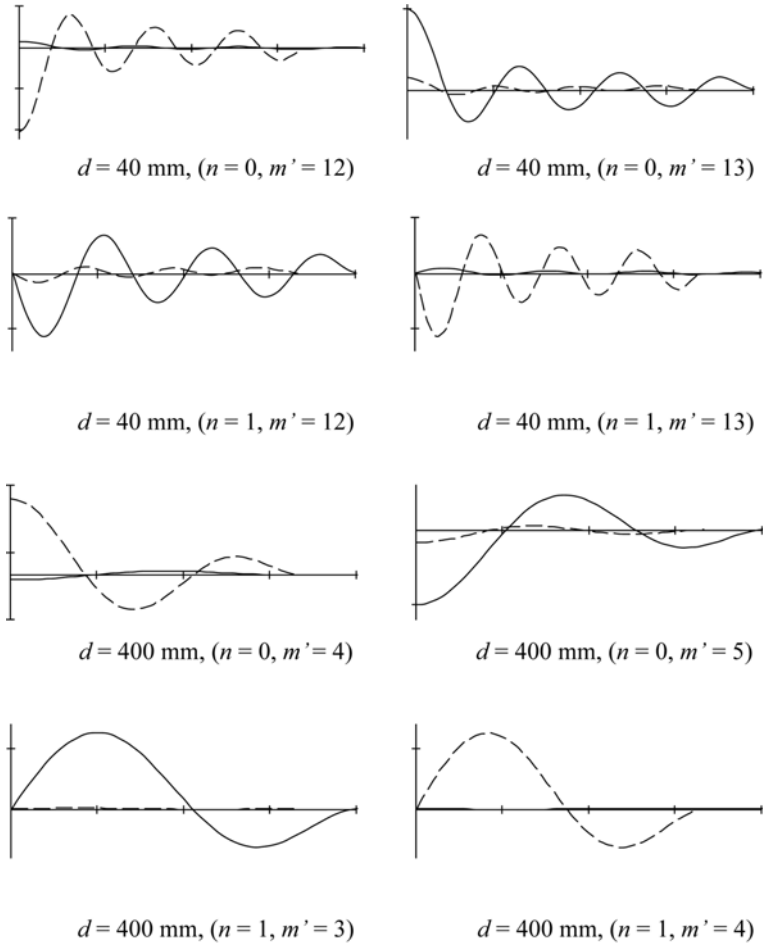

Fig. 3 Mode localization of two unequal aluminum circular plates coupled with water (—— ; upper plate, ---- ; lower plate)

localization and frequency loci veering phenomena were observed in some simple vibration systems (Kim 1998, Liu and Chan 1999, Liu 2002). The mode localization was also observed in the hydroelastic vibration of two circular cylindrical shells coupled with a fluid (Jeong 1998). By the same token, the mode localization appears in the free vibration of two circular plates coupled with a fluid. Fig. 3 shows two categories of the typical mode localization. The first four modes of Fig. 3 correspond to the first category which has a higher mode number and a relatively narrow fluid gap (d = 40 mm). The other four correspond to the second category and they have a lower mode number and a wide fluid gap (d = 400 mm). The first mode with m' = 12 and n = 0 in Fig. 3 shows that the modal displacement mainly takes place at the lower plate, but the second mode with m' = 13 and n = 0 at the upper plate. As the vibration modes increase, the hydrodynamic coupling effect gradually decreases owing to the dispersal (separation) effect of the fluid (Jeong and Lee 1998). Therefore the main fluid oscillates near only one plate at the higher modes. It is observed that the mode localization happens alternately at the upper and the lower plates as the number of the modes

increases. Because of this reason, the mode localization happens at the higher modes when the fluid gap is small.

On the other hand, the mode localization can also take place in the relatively lower modes since the hydroelastic coupling effect is remarkably reduced according to an increase of the distance between the plates such as the 5th~8th modes of Fig. 3. These vibration modes correspond to $m' = 4$ or 5 for $n = 0$, and $m' = 3$ or 4 for $n = 1$ when $d = 400$ mm. If the distance is large enough to diminish the fluid coupling, it seems that the two plates behave in such a manner that they independently float on an infinite fluid.

4.2 Natural frequency loci veering

Figs. 4 and 6 show the natural frequencies of the two circular plates with $R_1 = R_2 = a$ for $n = 0$ and $n = 1$ respectively as a function of the thickness difference factor. The thickness difference factor is defined as $|h_1 - h_2|/(h_1 + h_2)$ where the sum of the plate thickness $h_1 + h_2$ is taken as a constant.

When the difference factor is zero or in the identical plates case, the natural frequency 'A1' in Fig. 4 corresponds to the fundamental in-phase mode. As the difference in the plates thickness increases, the fundamental frequency decreases as indicated by 'A1'~'A6'. The first mode gradually

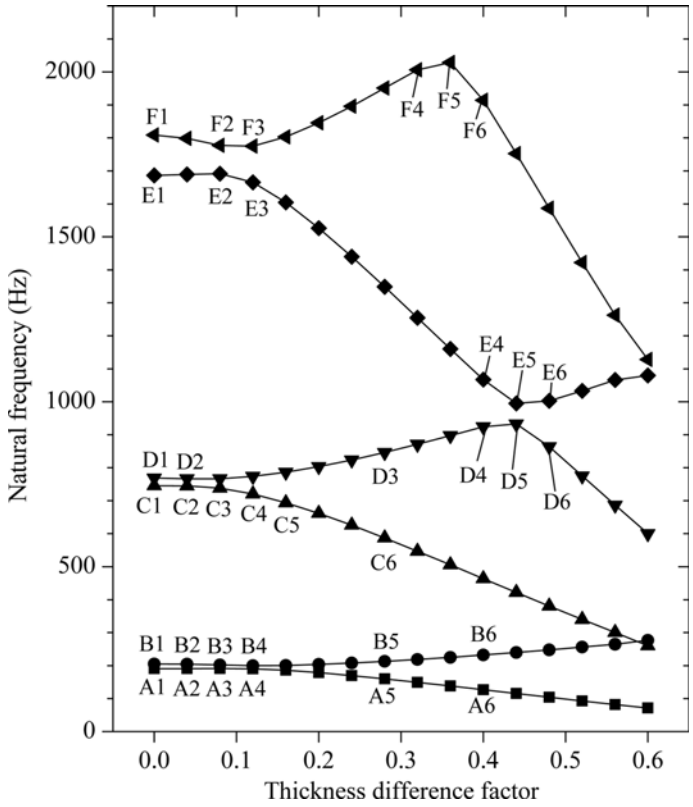

Fig. 4 Curve veering of the natural frequencies of two unequal circular plates coupled with water according to a plate thickness variation for $n = 0$, $d = 15$ mm and $R_1 = R_2 = a = 150$ mm

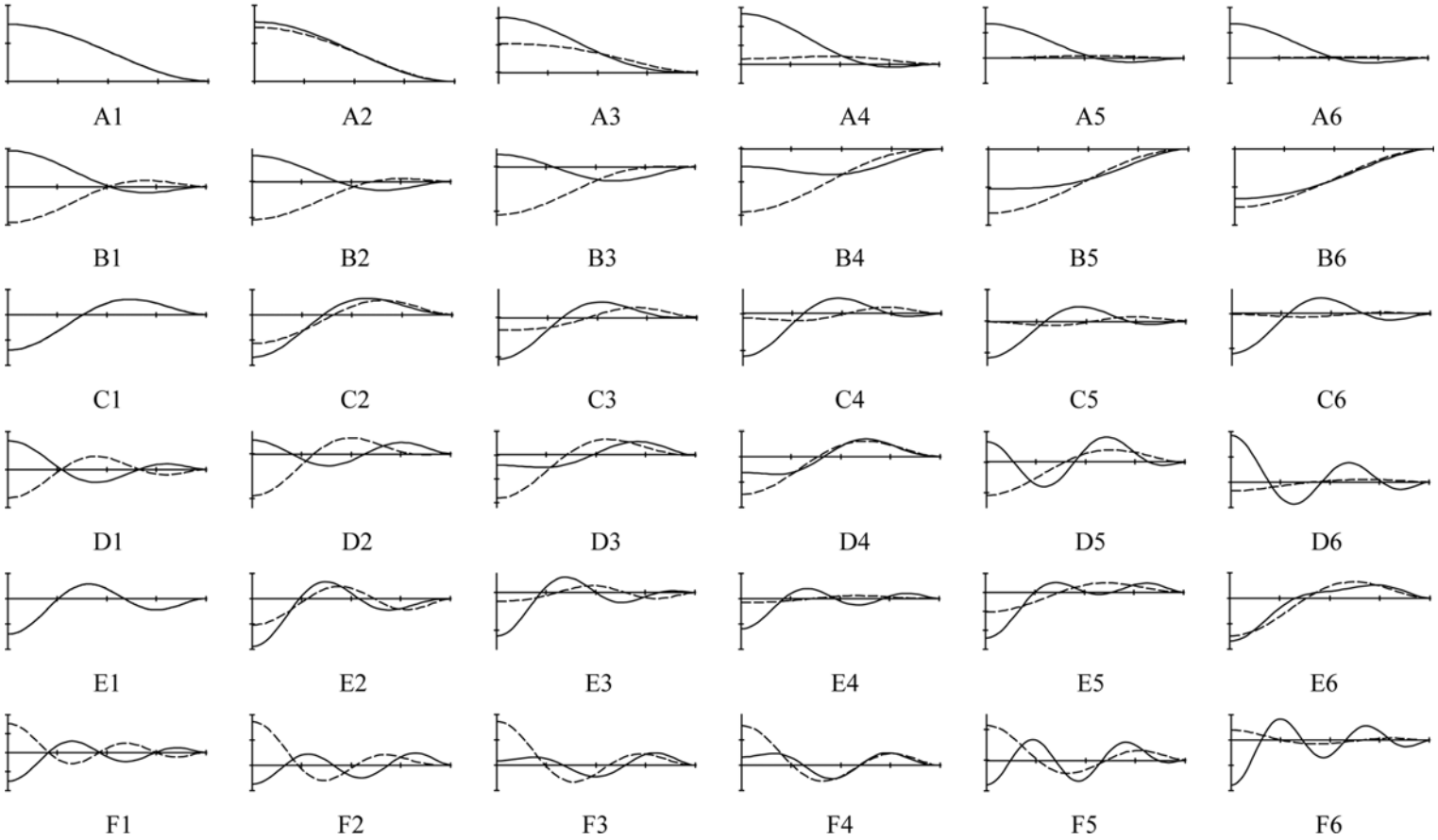

Fig. 5 Change of the mode shapes according to the thickness difference factor for $n = 0$ (——; upper plate, ----; lower plate)

changes from a symmetric in-phase mode to a psudo-symmetric in-phase mode with the thickness difference factor, and it eventually converges to a mode when the stiff plate has a considerably small displacement and the flexible plate has one nodal circle so that the fluid volume conservation requirement can be satisfied (A6 of Fig. 5). The second mode of Figs. 4 and 5 initiates from the out-of-phase mode (B1) with a nodal circle and the natural frequency gradually increases with the thickness difference factor. The mode moves to an in-phase mode (B6 of Figs. 4 and 5) when the thickness difference factor increases. The second mode shape (B6) resembles the in-phase mode (A2) of the first mode. The third mode of Fig. 4 starts from the in-phase mode (C1) with a nodal circle. As the thickness difference factor increases, the natural frequency decreases and the mode shape gradually changes to a mode (C6), which has a small deflection at the lower plate and two nodal circles at the upper plate. The fourth mode of Fig. 4 initiates from the out-of-phase mode (D1) with two nodal circles. The natural frequency increases to the point 'D4' which corresponds to the in-phase mode, and after the inflection point 'D5', the natural frequency abruptly decreases. The symmetric mode shape with two nodal circles dramatically changes near the inflection point as illustrated from 'E4' to 'E6' of Fig. 5 and the corresponding natural frequency locus also abruptly changes as shown in Fig. 4. After 'D5', the locus of the 4th mode looks like it has extended from the adjacent 5th mode locus near the two inflection points 'D5' and 'E5' in Fig. 4. Therefore at a first glance the two loci seem to be crossed. But, in fact, the loci do not encounter each other.

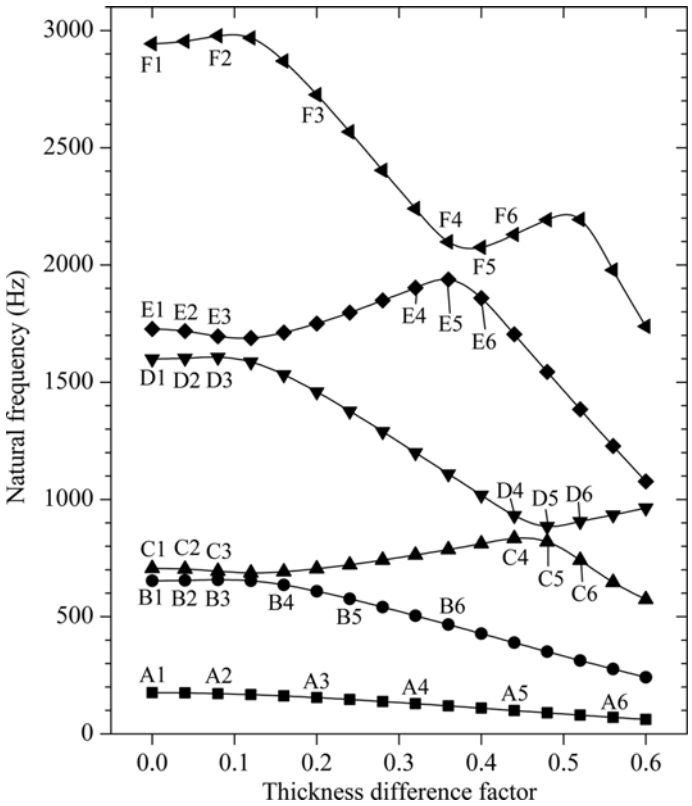

Fig. 6 Curve veering of the natural frequencies of two unequal circular plates coupled with water according to a plate thickness variation for $n = 1$, $d = 15$ mm and $R_1 = R_2 = a = 150$ mm

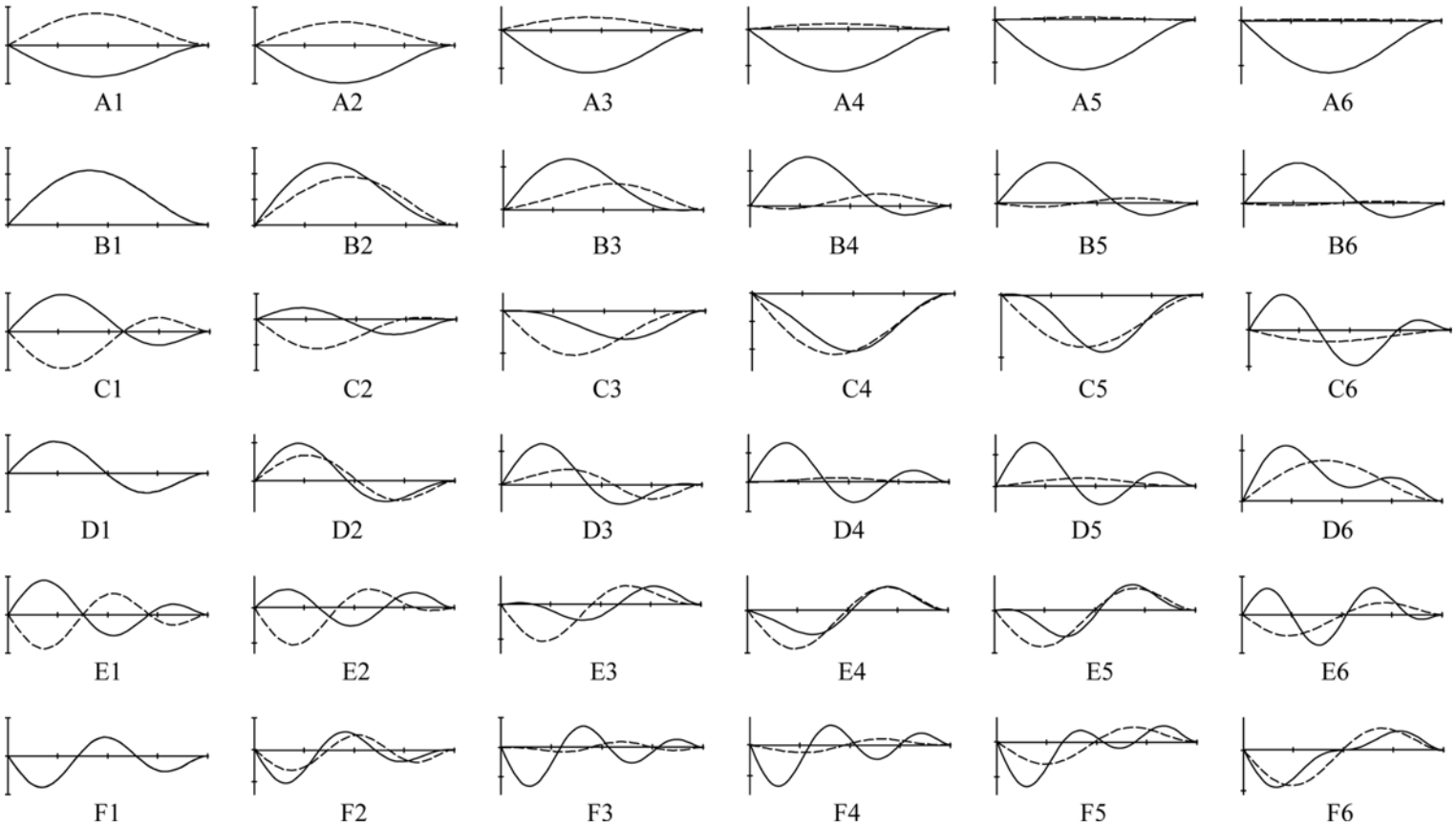

Fig. 7 Change of the mode shapes according to the thickness difference factor for n = 1 (——; upper plate, ----; lower plate)

Similar results can be observed in Figs. 6 and 7 for $n = 1$.

At this pint, let's summarize these two points. One is a relationship between the slope of the frequency loci and the mode shapes. When the in-phase mode shape shifts to an out-of-phase mode or a localized mode, the corresponding natural frequency tends to decrease, and vice versa. The other is the fact that similar mode shapes with different natural frequencies can be repeated in the higher modes when the thickness difference factor increases.

Figs. 8 and 10 plot the loci of the coupled natural frequencies of the two circular plates with an unequal thickness and $R_1 = R_2 = a$ for $n = 0$ and $n = 1$ respectively as a function of the distance between the plates. The figures also show the loci of the natural frequencies as a curve veering one. As the distance between the plates increases at the first mode, the natural frequency gradually increases and the out-of-phase mode (A1 of Fig. 9) with one nodal circle is converted to an in-phase mode (A6 of Fig. 9) with a zero nodal circle as illustrated in Fig. 8. The second mode starts from the out-of-phase mode shape (B1 of Fig. 9) with two nodal circles and changes to an in-phase mode shape (B3 of Fig. 9) with a zero nodal circle. Eventually it moves to a mixed mode (B6) with a zero nodal circle at the upper plate and with one nodal circle at the lower plate. The natural frequency increases to the inflection point and it finally decreases as the fluid gap increases. One of the remarkable observations is that the fundamental mode shape for $n = 1$ does not change regardless of the fluid gap as shown in Fig. 11. It is apparent that the complicated mode shape can

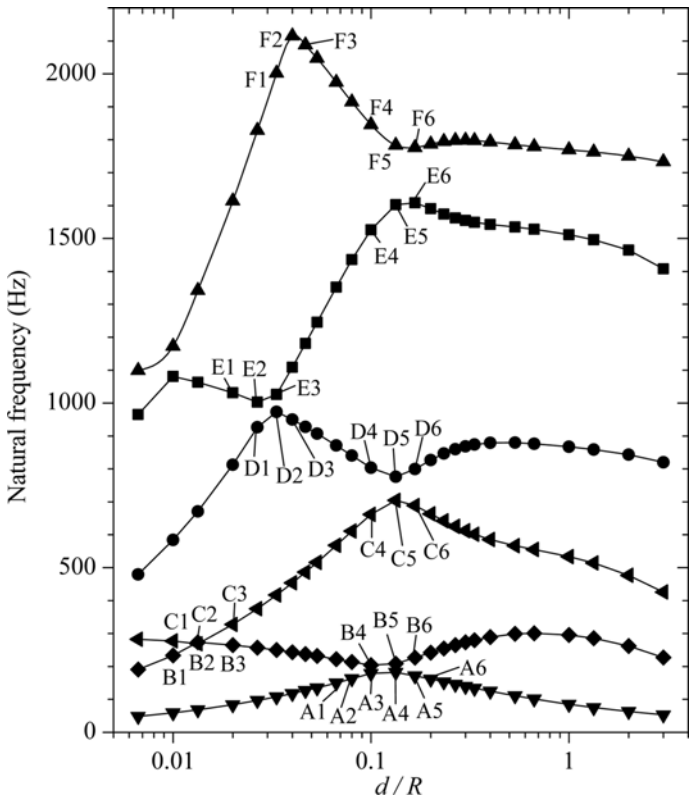

Fig. 8 Curve veering of the natural frequencies of two unequal circular plates coupled with water according to a distance between the plates for $n = 0$, $h_1 = 3$ mm, $h_2 = 2$ mm and $R_1 = R_2 = a = 150$ mm

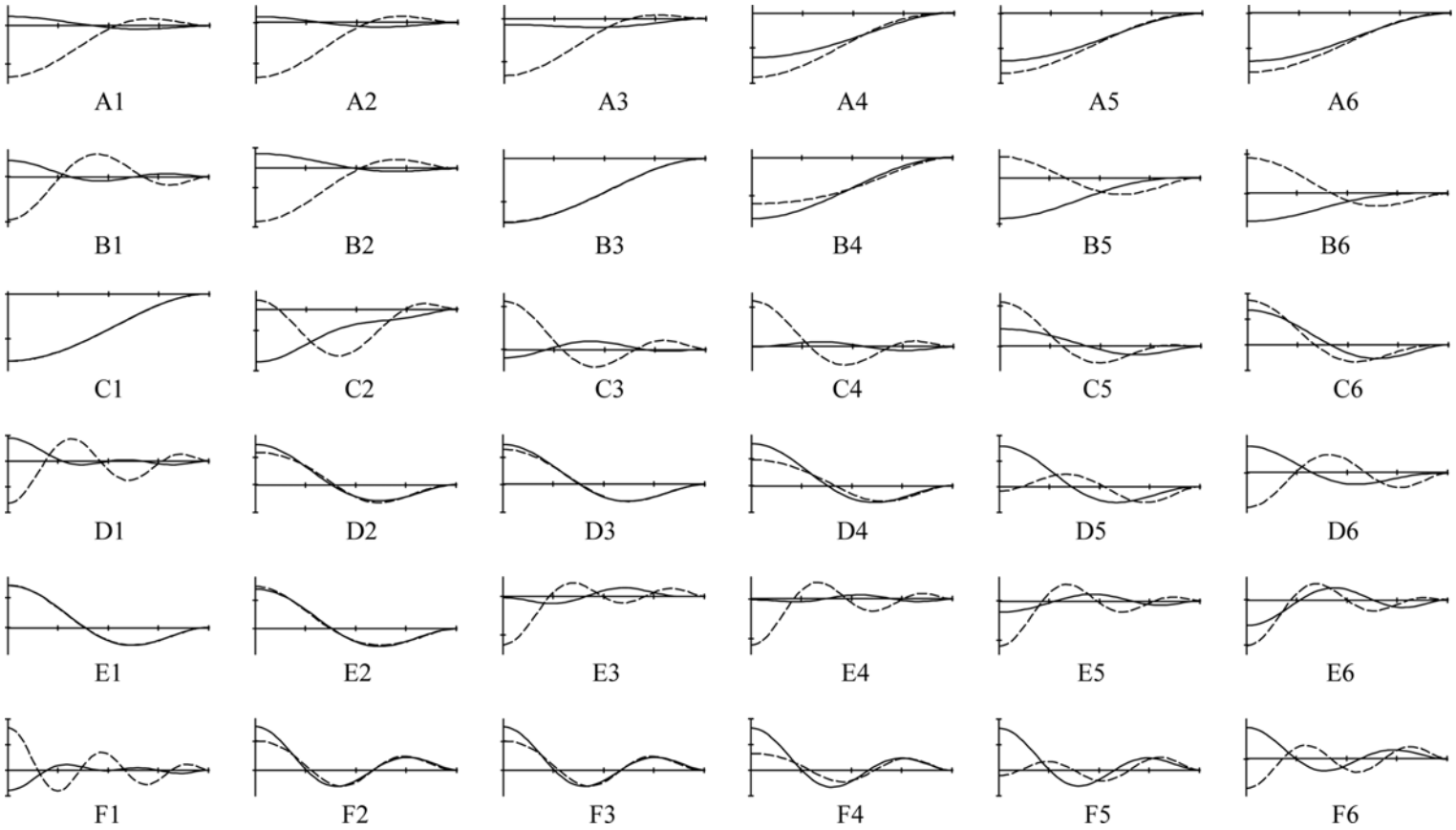

Fig. 9 Change of the mode shapes according to the distance between the plates for $n = 0$ (——; upper plate, ----; lower plate)

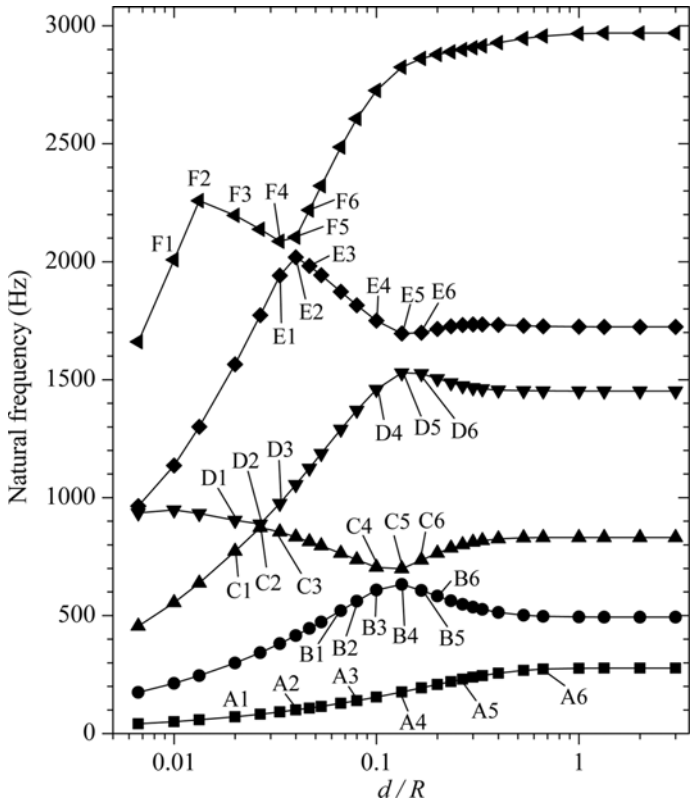

Fig. 10 Curve veering of the natural frequencies of two unequal circular plates coupled with water according to a distance between the plates for $n = 1$, $h_1 = 3$ mm, $h_2 = 2$ mm and $R_1 = R_2 = a = 150$ mm.

be shifted to a simple mode shape and it can also return to a complex mode shape again as shown in Figs. 9 and 11 as the fluid gap increases.

5. Conclusions

An analytical method to estimate the natural frequencies of two unequal circular plates with an unequal thickness and diameter and coupled with an inviscid and compressible fluid is developed using the Rayleigh-Ritz method. It is verified that the proposed theoretical approach can predict the coupled natural frequencies well. The following was observed in the present work:

1. The veering of the natural frequency loci curve and the mode localization phenomena appear in the system by increasing the distance of the plates and the thickness difference factor.
2. The natural frequency decreases when the in-phase mode shape shifts to the out-of-phase mode during a veering of the natural frequency loci curve, and vice versa.
3. The mode shape of two circular plates coupled with a fluid abruptly changes near the inflection point of the locus of the corresponding natural frequency.

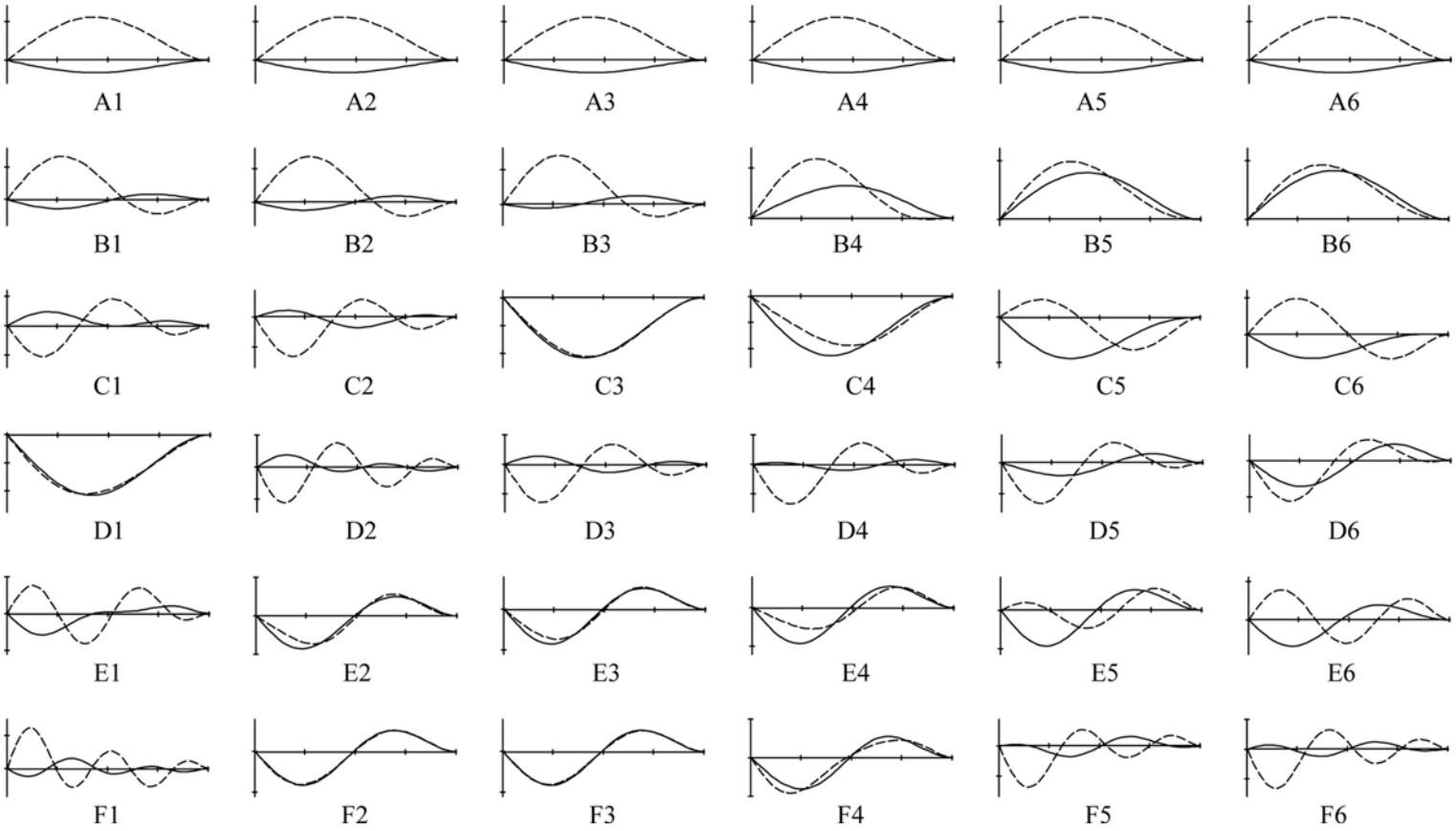

Fig. 11 Change of the mode shapes according to the distance between the plates for $n = 1$ (——; upper plate, ----; lower plate)

References

Amabili, M. (1995), "Free-edge circular plates vibrating in water", *Modal Analysis*: *The Int. J. of Analytical and Experimental Modal Analysis*, **10**, 187-202.

Amabili, M. (1996), "Effect of finite fluid depth on the hydroelastic vibrations of circular and annular plates", *J. Sound Vib.*, **193**, 909-925.

Amabili, M. and Kwak, M.K. (1999), "Vibration of circular plates on a free fluid surface: Effect of surface waves", *J. Sound Vib.*, **226**, 407-424.

Amabili, M. (2000), "Vibrations of fluid-filled hermetic cans", *J. of Fluids and Struct.*, **14**, 235-255.

Amabili, M. (2001), "Vibrations of circular plates resting on a sloshing liquid: Solution of the fully coupled problem", *J. Sound Vib.*, **245**, 261-283.

Bauer, H.F. (1995), "Coupled frequencies of a liquid in a circular cylindrical container with elastic liquid surface cover", *J. Sound Vib.*, **180**, 689-704.

Cheung, Y.K. and Zhou, D. (2002), "Hydroelastic vibration of a circular container bottom plate using the Galerkin method", *J. of Fluids Struct.*, **16**, 561-580.

Chiba, M. (1994), "Axisymmetric free hydroelastic vibration of a flexural bottom plate in a cylindrical tank supported on an elastic foundation", *J. Sound Vib.*, **169**, 387-394.

Jeong, K.H. (1998), "Natural frequencies and mode shapes of two coaxial cylindrical shells coupled with bounded fluid", *J. Sound Vib.*, **215**, 105-124.

Jeong, K.H. (2003), "Free vibration of two identical circular plates coupled with bounded fluid", *J. Sound Vib.*, **260**, 653-670.

Jeong, K.H. and Lee, S.C. (1998), "Hydroelastic vibration of a liquid-filled circular cylindrical shell", *Comput. Structs.*, **66**, 173-185.

Jeong, K.H. and Kim, K.J. (2005), "Hydroelastic vibration of a circular plate submerged in a bounded compressible fluid", *J. Sound Vib.*, **283**, 153-172.

Kwak, M.K. (1991), "Vibration of circular plates in contact with water", *J. Appl. Mech.*, **58**, 480-483.

Kim, D.O. and Lee, I.W. (1998), "Mode localization in simply supported two-span beams of arbitrary span lengths", *J. Sound Vib.*, **213**, 952-961.

Kwak, M.K. (1997), "Hydroelastic vibration of circular plates", *J. Sound Vib.*, **201**, 293-303.

Kwak, M.K. and Kim, K.C. (1991), "Axisymmetric vibration of circular plates in contact with fluid", *J. Sound Vib.*, **146**, 381-389.

Kwak, M.K. and Han, S.B. (2000), "Effect of fluid depth on the hydroelastic vibration of free-edge circular plate", *J. Sound Vib.*, **230**, 171-185.

Liu, J.K. and Chan, H.C. (1999), "Mode localization and frequency loci veering in an aircraft with external stores", *Struct. Eng. Mech.*, **8**, 181-191.

Liu, X.L. (2002), "Behavior of derivatives of eigenvalues and eigenvectors in curve veering and mode localization and their relation to close eigenvalues", *J. Sound Vib.*, **256**, 551-564.

Perkins, N.C. and Mote Jr., C.D. (1986), "Comments on curve veering in eigenvalue problems", *J. Sound Vib.*, **106**, 451-463.

Pierre, C. (1988), "Mode localization and eigenvalue loci veering phenomena in disordered structures", *J. Sound Vib.*, **126**, 485-502.

Pierre, C. and Dowell, E.H. (1987), "Localization of vibrations by structural irregularity", *J. Sound Vib.*, **114**, 549-564.